

Contents lists available at ScienceDirect

# Mechanical Systems and Signal Processing

journal homepage: [www.elsevier.com/locate/ymssp](http://www.elsevier.com/locate/ymssp)



## Integral terminal sliding-mode-based adaptive integral backstepping control for precision motion of a piezoelectric ultrasonic motor



Zhao Feng <sup>a,b</sup>, Wenyu Liang <sup>b,c,\*</sup>, Jie Ling <sup>a</sup>, Xiaohui Xiao <sup>a,\*</sup>, Kok Kiong Tan <sup>b</sup>, Tong Heng Lee <sup>b</sup>

<sup>a</sup>School of Power and Mechanical Engineering, Wuhan University, Wuhan 430072, China

<sup>b</sup>Department of Electrical and Computer Engineering, National University of Singapore, Singapore 117576, Singapore

<sup>c</sup>Institute for Infocomm Research (I2R), A\*STAR, Singapore 138632, Singapore

### ARTICLE INFO

#### Article history:

Received 5 November 2019

Received in revised form 27 February 2020

Accepted 28 March 2020

Available online 19 April 2020

#### Keywords:

Piezoelectric ultrasonic motor  
Integral terminal sliding surface  
Adaptive backstepping control  
Precision motion tracking

### ABSTRACT

The versatile and effective piezoelectric ultrasonic motor (PUM) has been widely used in many significant industrial and scientific applications, including precision positioning systems and surgical devices. However, the inherent friction, hysteresis nonlinearity, model uncertainties as well as various invariably presented external disturbances bring great challenges on the precision motion of PUM. In this development, a novel integral terminal sliding-mode-based adaptive integral backstepping control (ITSMAIBC) is formulated to accommodate these adverse impacts and retain high tracking precision. In particular, the second-order auxiliary differential equations based on the integral terminal sliding-mode surface are constructed to obtain the property of finite-time convergence and desired steady-state performance. Through employing integral backstepping methodology with the auxiliary equations, the asymptotic stability is guaranteed and a high-order sliding-mode control (SMC)-like performance is also achieved to relieve the chattering phenomenon. An adaptive law is further incorporated into the proposed controller to estimate the upper bound of the total disturbance. The robust stability is proven by the Lyapunov theory. Moreover, the implementation of ITSMAIBC is simple without any high-order derivative or observer. The actual experiments on a PUM verify the effectiveness of the controller through tracking continuous sinusoidal waves and discontinuous triangular waves with different frequencies and amplitudes, and the proposed scheme achieves the best tracking performance in comparison with three benchmark controllers. A surgical operation on a mock membrane experimental system is also performed to validate the practical application of the proposed method on ear surgery.

© 2020 Elsevier Ltd. All rights reserved.

## 1. Introduction

Precision motion with a resolution at micrometer or nanometer is a crucial aspect in the area of industrial and scientific applications, such as atomic force microscopes [1], dexterous micro manipulation [2], fast tool servo system [3], and so on. Therefore, piezoelectric-actuated devices have been developed widely in order to achieve the anticipated performance for their advantages of fast response time, high stiffness, compact structure, and high resolution [4,5]. Among these, to achieve

\* Corresponding authors at: School of Power and Mechanical Engineering, Wuhan University, Wuhan 430072, China (W. Liang).

E-mail addresses: [liangwenyu@nus.edu.sg](mailto:liangwenyu@nus.edu.sg) (W. Liang), [xhxiao@whu.edu.cn](mailto:xhxiao@whu.edu.cn) (X. Xiao).

fast motion speed as well as large stroke simultaneously, the piezoelectric ultrasonic motor (PUM) has been designed and used successfully in precision positioning system [6], and medical devices [7,8], showing great potential in practical applications.

The PUM generates high-speed linear motion through a slider in coupling with a pretensioned stator, which is driven by a piezoelectric actuator. The output of the piezoelectric actuator exerts pressure on the stator so that the resulted frictional force between the slider and stator can drive the stage with theoretically unlimited travel distance [9]. According to the driving principle of PUM, the challenges mainly stem from the produced friction in order to achieve the precision motion. Furthermore, the heat generated by the PUM with the increase of motion time or speed, and the inherent hysteresis can also lead to an adverse impact on the final motion accuracy.

In order to compensate the inaccuracy giving rise by the hysteresis nonlinearity, the model-based feedforward technologies have been widely used with the established hysteresis models, including Bouc-Wen model [10], Preisach model [11], Prandtl-Ishlinskii model [12] and so on. Furthermore, the Coulomb model [13], LuGre model [14], and Generalized Maxwell-Slip (GMS) model [15] also have been developed to describe and compensate the frictional force. However, to obtain the accurate descriptions and subsequently compensate the hysteresis and friction nonlinearities, lots of the model parameters should be identified off-line or on-line, and the processes are time-consuming and complicated for practical applications [16].

The intricate modeling process of hysteresis and friction can be avoided by the disturbance observer (DOB) methodology [17]. In [18], a frequency-domain DOB integrated with repetitive control was designed to compensate hysteresis and unknown disturbances. A sliding-mode-based DOB for motion tracking control of PUM was proposed to deal with the adverse effects in [19]. A nonlinear friction observer was designed to estimate viscous and Coulomb friction with application to rotary actuator with passive mechanical load in [20]. In [21], an extended state observer (ESO) and neural network control were used to cancel disturbances and approximate unknown function for a piezoelectric actuator-based surgical device. However, it is worth noting that these DOB-based methods are generally in cooperation with other tracking controllers to improve the overall performance, which increases the computation load for real-time implementation.

The additional DOB can be removed for these controllers with high robustness. Alternatively, sliding-mode control (SMC) provides effective and robust performance through taking the complex hysteresis and friction as external disturbances. In [22], the hysteresis nonlinearity was mitigated by an output-based discrete-time SMC without any observer, and a proportional-integral-derivative (PID) based SMC was proposed to eliminate the chattering problem in [23]. Furthermore, in [24], an adaptive SMC with a nonlinear observer was developed for the PUM in the presence of friction, hysteresis as well as unknown system parameters. To further improve the robustness to external disturbance and achieve globally asymptotic stability, the backstepping methodology based on the Lyapunov criterion have been combined with SMC in some studies. In [25], the backstepping technique was used to tackle the nonlinearity and the cross-couplings of a two-degrees-of-freedom piezoelectric actuator. Besides, an integral backstepping SMC with a recurrent neural network was developed for a piezo-flexural nanopositioning stage in [26] and a sliding-mode DOB-based adaptive integral backstepping control was proposed to achieve high precision tracking for a piezoelectric nano-manipulator in [27]. However, the bandwidth of DOB also limits the anticipated performance of the system with fast motion. Although the above methods improve the motion precision to some extent, the chattering phenomenon and finite-time convergence, which are vital to tracking performance, are not taken into consideration.

The finite-time convergence can be guaranteed by selecting proper sliding function [28] and the chattering phenomenon will be alleviated by integrating with DOB [29] or high-order SMC [30]. In [31], an adaptive backstepping nonsingular fast terminal SMC was proposed to increase the tracking performance of the robot manipulator. It is found that the singular value may occur in the control force if the derivative of error equals to zero, and only the simulation results are provided.

Motivated by aforementioned essential issues, a novel integral terminal sliding-mode-based adaptive integral backstepping control (ITSMAIBC) is proposed to achieve high precision and fast motion in this paper for a PUM, where complex hysteresis and friction nonlinearities, unknown heat disturbance, model uncertainties, and other external disturbance are presented. The model of the system dynamics is firstly built. Next, the design of the proposed ITSMAIBC is given in detail, and the system stability is analyzed by the Lyapunov theory. Then, the effectiveness of ITSMAIBC is also examined on the PUM through comparative experiments with different reference scenarios, which test the feasibility of practical application. Finally, the method is carried out on a surgical device to complete the surgical operation. The implementation of the proposed control method is simple for practical application with the merits of no disturbance or state observer including in the control scheme, and high robustness to hysteresis and friction nonlinearities, unknown disturbances as well as parameters' uncertainties. The main contributions of this paper are listed below.

- A novel second-order auxiliary differential equations based on integral terminal sliding function with the position error is proposed in this paper firstly. Being different from the PID-type [32] or conventional terminal [33] sliding mode function, the auxiliary equations ensure the finite-time convergence performance as well as better tracking performance through the integral action [34], and provide the foundation to deduce the proposed new and better performing control law.

- A new integral backstepping methodology with the Lyapunov criterion based on the auxiliary differential equations is utilized to make the sliding function and its time derivative to converge to zero so that the high-order SMC-like performance and globally asymptotic stability are guaranteed. Furthermore, the integral actions of the virtual variables are augmented in the control scheme to improve the steady-state performance and robustness, and the adaptive control law is designed to estimate the upper bound of the total disturbance to further relieve chattering phenomenon.
- Detailed discussions on the proposed control scheme performance are conducted via theoretical analysis as well as extensive and comparative experiments with different conditions to illustrate the superior performance of the proposed method on the PUM, which presents significantly adverse impacts on tracking precision. The surgical operation on mock membrane are also tested to validate the practical application of the proposed method for the ear surgery.

The remainder of this paper is structured as follows. The model of the PUM is established in Section 2. The proposed ITS-MAIBC and the stability analysis are presented in Section 3. Section 4 gives the detailed experimental and implementation of the controllers. Experiments on a PUM and comparisons of the results are elaborated in Section 5 and Section 6 gives the conclusions.

## 2. Model of the Piezoelectric ultrasonic motor

The linear part of piezoelectric-actuated devices can be modeled as a second-order system generally [29,35]. Taking the hysteresis, friction, and external disturbances into consideration, a diagram for the model of PUM is given in Fig. 1, which can be represented as

$$m\ddot{x} + b\dot{x} + kx + f_c + f_h + f_{ed} = Tu, \quad (1)$$

where  $m, b, k$  are the effective mass, damping and stiffness parameters.  $x$  is the output position of PUM,  $\dot{x}$  and  $\ddot{x}$  are the velocity and acceleration, respectively. Furthermore, the input voltage to the piezoelectric actuator is denoted as  $u$  through a electromechanical ratio  $T$  of the system.  $f_c$  and  $f_h$  represent the friction and hysteresis nonlinearities, respectively, and  $f_{ed}$  are the unknown disturbances, such as heat and external disturbances which always exist in such system.

**Assumption 1** [21,25,36] The  $f_c, f_h$  and  $f_{ed}$  are bounded and satisfy the following conditions,

$$|f_c| \leq \Theta_c, |f_h| \leq \Theta_h, |f_{ed}| \leq \Theta_{ed}, \quad (2)$$

where  $\Theta_c, \Theta_h, \Theta_{ed}$  are positive constants.

However, the accurate parameters of  $m, b, k$  are difficult to be obtained in practice. In this paper, the nominal or identified parameters  $m_n, b_n, k_n$  are defined to facilitate the controller design with the following relationships,

$$m = m_n + \Delta m, b = b_n + \Delta b, k = k_n + \Delta k, \quad (3)$$

where  $\Delta m, \Delta b, \Delta k$  are the model uncertainties of the PUM with the upper bounds of  $\Theta_m, \Theta_b, \Theta_k$ , respectively. Therefore, the system (1) can be rewritten as

$$m_n\ddot{x} + b_n\dot{x} + k_nx + \Delta m\ddot{x} + \Delta b\dot{x} + \Delta kx + f_c + f_h + f_{ed} = Tu, \quad (4)$$

**Assumption 2** [33] The model uncertainties  $\Xi = \Delta m\ddot{x} + \Delta b\dot{x} + \Delta kx$  are bound by

$$|\Xi| \leq \Theta_m|\ddot{x}| + \Theta_b|\dot{x}| + \Theta_k|x| = \Theta_\Xi, \quad (5)$$

where  $\Theta_\Xi$  is a positive constant.

Based on the above assumptions, the total disturbance  $f_t = \Delta m\ddot{x} + \Delta b\dot{x} + \Delta kx + f_c + f_h + f_{ed}$  is also bounded as

$$|f_t| \leq \Theta_{f_t} = \Theta_\Xi + \Theta_c + \Theta_h + \Theta_{ed}, \quad (6)$$

where  $\Theta_{f_t}$  is an unknown parameter. Thus, the dynamics of PUM is simplified and converted as

$$m_n\ddot{x} + b_n\dot{x} + k_nx + f_t = Tu. \quad (7)$$

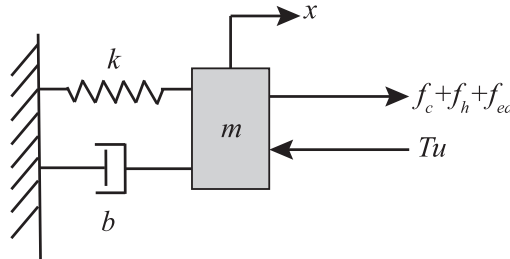


**Fig. 1.** A diagram for the model of PUM.

The objective of this paper is to track the desired trajectory  $x_d$  accurately without any disturbance/state observer at the presence of complex and unknown disturbance  $f_t$ .

**Remark 1.** In order to compensate the hysteresis or friction, the inverse compensators with different models, and compensation it as a bounded disturbance are the two most preferred, effective and used methods [16,37,38]. It should be noted that the accurate descriptions and subsequent compensation of the nonlinearities will involve the need to identify quite a large number of the related model parameters. Therefore, the effects arising from hysteresis, friction, model uncertainties and other disturbance are taken as bounded by positive values with the aim to attain an effective controller design in this paper. These assumptions have been widely used in piezoelectric-actuated devices in [21,25,33,36], where the unknown disturbances are treated as a total disturbance to avoid complex modeling of friction or hysteresis nonlinearity, and there always exists an upper bound for actual system. Therefore, the robustness of the designed controller to these adverse impacts is an important aspect to be taken into consideration in this paper.

### 3. Integral terminal sliding-mode-based adaptive integral backstepping control design

#### 3.1. Integral backstepping controller with integral terminal sliding function

Due to the complex and unknown disturbance like friction and hysteresis, it is a challenge to achieve precision motion tracking of PUM to meet the requirements of practical applications, such as surgical device [35]. Therefore, the goal of the proposed control scheme is to minimize the tracking error defined as

$$e = x - x_d. \quad (8)$$

To achieve finite-time convergence of the desired reference and minimize steady-state error, an integral terminal sliding function is adopted in this paper [28], which is defined as

$$\sigma = k_1 e + k_2 \int |e|^\alpha \text{sign}(e) dt. \quad (9)$$

Consider the Lyapunov candidate function

$$V_e = \frac{1}{2} e^2, \quad (10)$$

and its time derivative is given as

$$\dot{V}_e = \dot{e}e. \quad (11)$$

During the sliding motion,  $\dot{\sigma} = 0$  is produced, and thus  $\dot{e}$  is calculated as

$$\dot{e} = -\frac{k_2}{k_1} |e|^\alpha \text{sign}(e). \quad (12)$$

Then,  $\dot{V}_e$  becomes

$$\begin{aligned} \dot{V}_e &= -\frac{k_2}{k_1} |e|^\alpha \text{sign}(e)e = -\frac{k_2}{k_1} |e|^{(\alpha+1)} \\ &\leq -\frac{k_2}{k_1} (e^2)^{\frac{\alpha+1}{2}} = -\frac{2^{\frac{\alpha+1}{2}} k_2}{k_1} (\frac{e^2}{2})^{\frac{\alpha+1}{2}} = -\frac{2^{\frac{\alpha+1}{2}} k_2}{k_1} (V_e)^{\frac{\alpha+1}{2}} \leq 0. \end{aligned} \quad (13)$$

Therefore, we can obtain that

$$\dot{V}_e + \rho V_e^\eta \leq 0 \quad (14)$$

with  $\rho = \frac{2^{\frac{\alpha+1}{2}} k_2}{k_1}$ ,  $\eta = \frac{\alpha+1}{2}$ . In order to achieve finite-time convergence, it should be satisfied that  $\rho > 0$ ,  $0 < \eta < 1$  [39]. The parameters in (9) are chosen to meet the conditions of  $k_1 > 0$ ,  $k_2 > 0$ , and  $\frac{1}{2} < \alpha < 1$ , and it will converge in a finite time  $T_s$ , which is expressed as [28]

$$T_s \leq \frac{V_{e,0}^{1-\eta}}{\rho(1-\eta)}, \quad (15)$$

where  $V_{e,0}$  is the initial value of the Lyapunov candidate function (10).

Because (9) is continuous and differentiable, the derivative of the sliding function with respect to time is given as

$$\dot{\sigma} = k_1 \dot{e} + k_2 |e|^\alpha \text{sign}(e). \quad (16)$$

Then, the time derivative of (16) is represented as

$$\ddot{\sigma} = k_1 \ddot{e} + k_2 \alpha |e|^{\alpha-1} \dot{e} = k_1 \ddot{e} - \frac{\alpha k_2^2}{k_1} |e|^{2\alpha-1} \text{sign}(e). \quad (17)$$

Combining (16) with (17), the second-order auxiliary differential equations based on the integral terminal sliding-mode function are constructed as

$$\begin{cases} \dot{\sigma}_1 = \sigma_2 \\ \dot{\sigma}_2 = k_1 \ddot{e} - \frac{\alpha k_2^2}{k_1} |e|^{2\alpha-1} \text{sign}(e) \\ \sigma_1 = \sigma. \end{cases} \quad (18)$$

Based on (18), an integral backstepping methodology is employed to deduce the control law. To improve the steady-state performance of the sliding function, the integral action is augmented in the design process. Define the integration of  $\sigma_1$  as

$$\chi_1 = \int \sigma_1 dt. \quad (19)$$

In order to ensure the asymptotic stability of  $\sigma_1$ , the Lyapunov function candidate is chosen as

$$V_1 = \frac{1}{2} \sigma_1^2 + \frac{\lambda_1}{2} \chi_1^2, \quad (20)$$

where  $\lambda_1$  is a positive parameter. Then, we can get the time derivative of  $V_1$  as

$$\dot{V}_1 = \sigma_1 \dot{\sigma}_1 + \lambda_1 \chi_1 \dot{\chi}_1 = \sigma_1 \sigma_2 + \lambda_1 \chi_1 \sigma_1. \quad (21)$$

To make  $\dot{V}_1$  negative, i.e.,  $\dot{V}_1 < 0$ , according to (21), the desired  $\sigma_2$  should be given as

$$\phi = -\xi_1 \sigma_1 - \lambda_1 \chi_1, \quad (22)$$

where  $\phi = \sigma_2^d$  is the virtual variable, and  $\xi_1$  is a parameter to be designed. Furthermore, the error between  $\sigma_2$  and  $\sigma_2^d$  is defined as

$$z = \sigma_2 - \sigma_2^d = \sigma_2 - \phi. \quad (23)$$

Then, the above equation is rearranged as

$$\sigma_2 = z + \phi = -\xi_1 \sigma_1 - \lambda_1 \chi_1 + z. \quad (24)$$

Substituting (24) into (21), the time derivative of Lyapunov function  $V_1$  becomes

$$\dot{V}_1 = \sigma_1(-\xi_1 \sigma_1 - \lambda_1 \chi_1 + z) + \lambda_1 \chi_1 \sigma_1 = -\xi_1 \sigma_1^2 + \sigma_1 z. \quad (25)$$

Next, define the integral error  $z$  as

$$\chi_2 = \int z dt. \quad (26)$$

To make the error  $z$  as well as the integration of error converge to zero, the following Lyapunov function is proposed as

$$V_2 = V_1 + \frac{1}{2} z^2 + \frac{\lambda_2}{2} \chi_2^2, \quad (27)$$

where  $\lambda_2$  is a positive constant. The time derivative of  $V_2$  is deduced as

$$\dot{V}_2 = \dot{V}_1 + z \dot{z} + \lambda_2 \chi_2 \dot{\chi}_2. \quad (28)$$

Taking (25) and (26) into (28), we can have

$$\dot{V}_2 = -\xi_1 \sigma_1^2 + \sigma_1 z + \lambda_2 \chi_2 z + z \dot{z}. \quad (29)$$

**Theorem 1.** For the PUM system given by (7), the sliding function  $\sigma$ , virtual variable error  $z$  as well as the motion tracking error  $e$  will converge to zero if the following integral backstepping control law with the integral terminal sliding function (9) is satisfied,

$$\begin{cases} u = \frac{1}{T} [b_n \dot{x} + k_n x - \Upsilon \text{sign}(z)] + \frac{m_n}{T k_1} \\ [k_1 \ddot{x}_d + \frac{\alpha k_2^2}{k_1} |e|^{2\alpha-1} \text{sign}(e) + \dot{\phi} - \lambda_2 \chi_2 - \xi_2 z - \sigma_1]. \end{cases} \quad (30)$$

where  $\xi_2$  is a positive constant, and  $\Upsilon$  is the switching gain that satisfies the follow condition,

$$\Upsilon > \Theta_{f_t}. \quad (31)$$

**Proof of Theorem 1.** From (29) and in combination with (23), it is obtained that

$$\dot{V}_2 = -\xi_1 \sigma_1^2 + \sigma_1 z + \lambda_2 \chi_2 z + z(\dot{\sigma}_2 - \dot{\phi}). \quad (32)$$

Substitute (18) into the above equation,

$$\dot{V}_2 = -\xi_1 \sigma_1^2 + \sigma_1 z + \lambda_2 \chi_2 z + z[k_1 \ddot{e} - \frac{\alpha k_2^2}{k_1} |e|^{2\alpha-1} \text{sign}(e) - \dot{\phi}]. \quad (33)$$

From (7), the dynamics of PUM can be transformed into

$$\ddot{x} = \frac{1}{m_n}(-b_n \dot{x} - k_n x + Tu - f_t) \quad (34)$$

and taking  $\ddot{e} = \ddot{x} - \ddot{x}_d$  into (33), it becomes

$$\dot{V}_2 = -\xi_1 \sigma_1^2 + \sigma_1 z + \lambda_2 \chi_2 z + z \left[ \frac{k_1}{m_n} (-b_n \dot{x} - k_n x + Tu - f_t) - k_1 \ddot{x}_d - \frac{\alpha k_2^2}{k_1} |e|^{2\alpha-1} \text{sign}(e) - \dot{\phi} \right]. \quad (35)$$

Substitute the control law (30) into (35), leading to

$$\dot{V}_2 = -\xi_1 \sigma_1^2 - \xi_2 z^2 - \frac{k_1}{m_n} (\Upsilon |z| + f_t z). \quad (36)$$

If (31) is satisfied, the final  $\dot{V}_2$  meets the following inequality,

$$\dot{V}_2 < -\xi_1 \sigma_1^2 - \xi_2 z^2 \leq 0, \quad (37)$$

which shows that  $\dot{V}_2$  is negative definite, implying that  $\sigma_1$  and  $z$  will decay to zero with the proposed control law. Therefore, based on  $\sigma \rightarrow 0$ ,  $\dot{\sigma} \rightarrow 0$ , the position error will also converge in a finite time after the system reaches the sliding mode [40,41]. This completes the proof. ■

### 3.2. Adaptive control law design

According to the control input given in (30) and (31), the parameter  $\Upsilon$  should be determined in advance based on the upper bound of the total disturbance  $\Theta_{f_t}$ . In practice, the disturbances, including friction, hysteresis, and heat disturbance are time-varying and complex so that the upper bound is difficult to be obtained. Therefore, to retain the robust stability,  $\Upsilon$  is always given a relatively larger value. However, this conservative method may result in chattering vibration on the control force and deteriorating the tracking performance subsequently. In this paper, an adaptive methodology is utilized to alleviate the problem. To estimate the upper bound of disturbance, the estimated error is defined as

$$\tilde{\Upsilon} = \hat{\Upsilon} - \Upsilon. \quad (38)$$

**Theorem 2.** For the PUM system given by (7), the sliding function  $\sigma$ , virtual variable error  $z$  as well as the motion tracking error  $e$  will converge to zero if the control law of ITSMAIBC is selected as

$$\begin{aligned} u. = & \frac{1}{T} [b_n \dot{x} + k_n x - \hat{\Upsilon} \text{sign}(z)] + \frac{m_n}{T k_1} \\ & [k_1 \ddot{x}_d + \frac{\alpha k_2^2}{k_1} |e|^{2\alpha-1} \text{sign}(e) + \dot{\phi} - \lambda_2 \chi_2 - \xi_2 z - \sigma_1], \end{aligned} \quad (39)$$

with the adaptive law

$$\dot{\hat{\Upsilon}} = \frac{\gamma k_1}{m_n} |z|, \quad (40)$$

where  $\gamma$  is the adaptive gain.

**Proof of Theorem 2.** Consider the following Lyapunov function

$$V_3 = V_2 + \frac{1}{2\gamma} \tilde{\Upsilon}^2, \quad (41)$$

and its time derivation is given as

$$\dot{V}_3 = \dot{V}_2 + \gamma^{-1} \tilde{\Upsilon} \dot{\tilde{\Upsilon}}. \quad (42)$$

In combination with (35) and (38), we can deduce that

$$\begin{aligned} \dot{V}_3 = & -\xi_1 \sigma_1^2 + \sigma_1 z + \lambda_2 \chi_2 z + z \left[ \frac{k_1}{m_n} (-b_n \dot{x} - k_n x + Tu - f_t) \right. \\ & \left. - k_1 \ddot{x}_d - \frac{\alpha k_2^2}{k_1} |e|^{2\alpha-1} \text{sign}(e) - \dot{\phi} \right] + \gamma^{-1} (\hat{\Upsilon} - \Upsilon) \dot{\tilde{\Upsilon}}. \end{aligned} \quad (43)$$

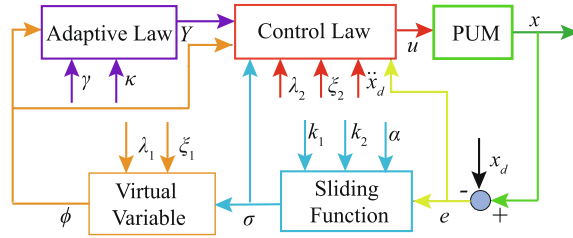


**Fig. 2.** Block diagram of the proposed ITSMAIBC scheme.

Substituting the control law of ITSMAIBC, i.e., (39) and (40), into  $\dot{V}_3$ , yields

$$\begin{aligned}\dot{V}_3 &= -\xi_1 \sigma_1^2 - \xi_2 z^2 - \frac{k_1}{m_n} (\hat{\Upsilon}|z| + f_t z) + \gamma^{-1} (\hat{\Upsilon} - \Upsilon) \frac{\gamma k_1}{m_n} |z| \\ &= -\xi_1 \sigma_1^2 - \xi_2 z^2 - \frac{k_1}{m_n} (\Upsilon|z| + f_t z) \\ &< -\xi_1 \sigma_1^2 - \xi_2 z^2,\end{aligned}\quad (44)$$

which shows that  $\dot{V}_3$  is negative definite. The sliding function  $\sigma, z$  presented asymptotic stability according to (44). Denote  $T_r$  as the time for any initial state  $\sigma \neq 0, \dot{\sigma} \neq 0$  converge to zero. After that the tracking error will converge to zero as a consequence according to (9). Therefore, the total time for the state in the sliding function to zero is within  $T_f = T_r + T_s$  [40,41] based on (15).

Therefore, through the backstepping methodology, the globally asymptotic stability is guaranteed even in the presence of unknown disturbance, such as friction, hysteresis, and so on. This completes the proof. ■.

### 3.3. Overall control law

To avoid the drift problem when estimating the upper bound  $\hat{\Upsilon}$  with the update law (40), a dead-zone technique [42] is employed as shown below

$$\dot{\hat{\Upsilon}} = \begin{cases} 0, & \text{if } |z| \leq \kappa \\ \frac{\gamma k_1}{m_n} |z|, & \text{if } |z| > \kappa, \end{cases} \quad (45)$$

where  $\kappa$  is the dead zone boundary. Hence, the overall control law is given by

$$\begin{aligned}u &= \frac{1}{T} [b_n \dot{x} + k_n x - \hat{\Upsilon} \text{sign}(z)] + \frac{m_n}{T k_1} \\ &\quad [k_1 \ddot{x}_d + \frac{\alpha k_2^2}{k_1} |e|^{2x-1} \text{sign}(e) + \dot{\phi} - \lambda_2 \chi_2 - \xi_2 z - \sigma_1],\end{aligned}\quad (46)$$

with the modified adaptive law (45). The block diagram of the proposed ITSMAIBC scheme is given in Fig. 2.

**Remark 2.** In this paper, the hysteresis and friction are treated as disturbances together with other external adverse factors to avoid complex hysteresis identification in [18,43], friction estimation in [20]. Furthermore, for the high robustness to the external disturbance, no state observer or DOB methodology, such as ESO [21] and nonlinear observer [24] is incorporated into the proposed control scheme, which simplifies the implementation.

**Remark 3.** Compared with the conventional terminal sliding mode control [33,44], the integral action in (9) is very important to improve the transient and steady-state response [34]. Furthermore, the integral action in the backstepping control also make the integral errors of  $\sigma_1$  and  $\sigma_2$  converge to zero so that the robustness to external disturbance and tracking performance are further improved.

**Remark 4.** Different from the method proposed in [25,27], where the backstepping control law is deduced based on the tracking error directly, the proposed ITSMAIBC employs an integral terminal sliding manifold to realize finite-time convergence and well tracking performance. Furthermore, the integral backstepping control law is obtained by the sliding function-based differential equations and avoids the singular value in [31].

## 4. Experimental setup

### 4.1. Experimental system

The tracking performance is tested on the PUM (PI-M663, Physik Instrumente) for a surgical device developed in [35]. The experimental platform and the overall control system are illustrated in Fig. 3. The implementation of ITSMAIBC is based on

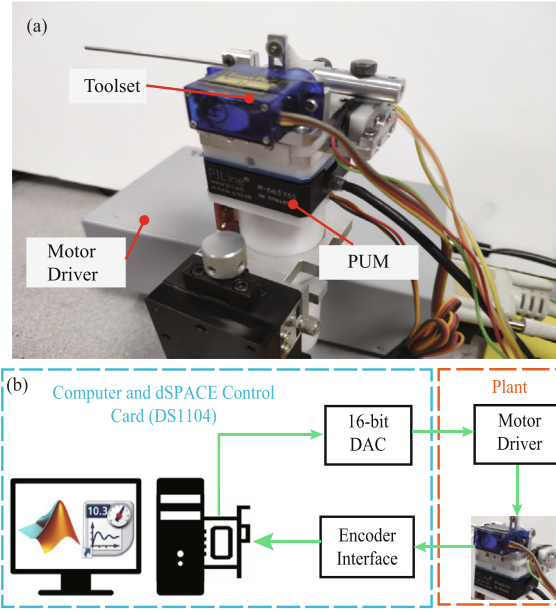


**Fig. 3.** The experimental setup of PUM. (a) experimental platform. (b) overall block diagram of control system.

the dSPACE control card (DS1104) through compiling the Simulink blocks developed in MATLAB. The input voltage between  $-10$  to  $+10$  V passed through a 16-bit digital-to-analogue converter (DAC) is amplified by the motor driver (C-867, Physik Instrumente) to drive the piezoelectric actuator. The measured position is sent to the control system through a linear encoder interface. The sample rate of the overall system is set as 1000 Hz. The nominal and linear part of PUM are identified through the input-output data excited by a multi-frequencies square wave to avoid the effect of nonlinearity. By virtual of MATLAB system identification toolbox, the nominal plant is described as

$$\ddot{x} + 248.4\dot{x} + 202x = 4940u. \quad (47)$$

The comparison of the measured position and identified result is plotted in Fig. 4. The model of (47) can capture the dynamics over 90%. It should be noted that the toolset for the surgery mount on the PUM is considered as a load uncertainty in this paper. Therefore, the model uncertainties of the system is actually more than 10% in practice. Moreover, the friction phenomenon is also obvious when sinusoidal waves with different amplitudes are injected into the open-loop system, as shown in Fig. 5. To overcome the static friction, the PUM can be actuated only when the input voltage is high enough, and the voltages are varied with the input amplitudes. Furthermore, the friction also present asymmetry with different motion direction as shown in Fig. 5. These factors bring serious challenges to control the PUM accurately, the controller should be robust enough to handle the problem.

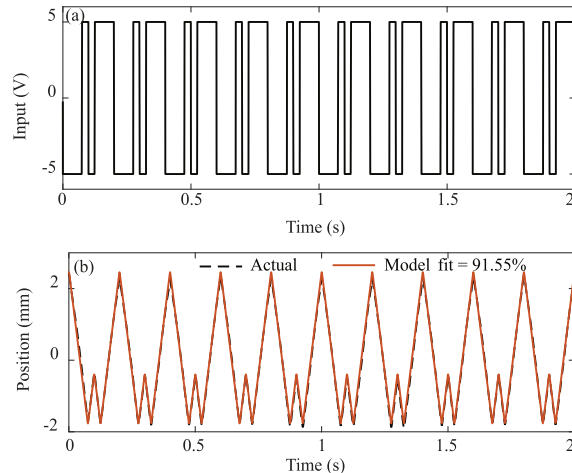


**Fig. 4.** Model validation of PUM. (a) input voltage. (b) comparison of the actual and identified output position.

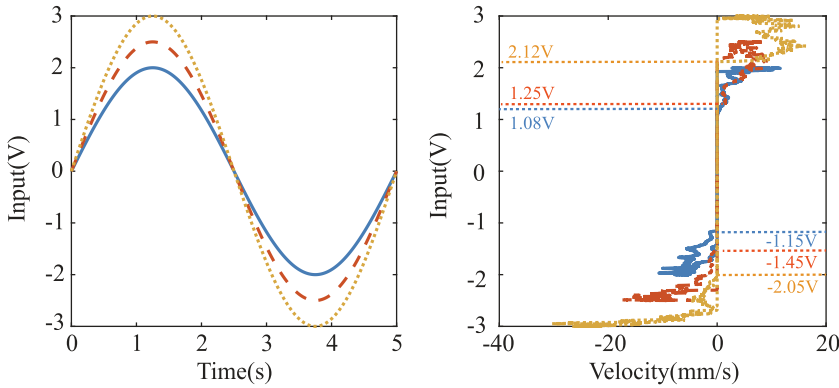


**Fig. 5.** An illustration of the friction phenomenon in PUM for sinusoidal saves with different amplitudes.

#### 4.2. Parameters of controllers

To highlight the performance of the proposed ITSMAIBC, another three controllers are also developed in this paper. To accommodate the disturbances of PUM, these controllers are added with an ESO to further improve the precision under unknown adverse impacts [45] and the estimated disturbance is denoted as  $\hat{d}$  with the observer bandwidth at 150 Hz.

(1) PID with ESO (PID + ESO): To get optimal parameters, the control gains are calculated by a linear-quadratic regulator (LQR) [35], the control input is given as

$$u_1 = -K_p e - K_i \int e dt - K_p \dot{e} - \hat{d}. \quad (48)$$

(2) Adaptive integral backstepping control (AIBC) with ESO (AIBC + ESO): The AIBC based on position error  $e$  is also given as a benchmark in this paper [27] and the observer is replaced by ESO for a fair comparison with the following control law,

$$u_2 = \frac{1}{T} [b_n \dot{x} + k_n x + m_n (\dot{\phi} - k_2 z - \lambda_2 \chi_2 - e) + \hat{F}] - \hat{d}, \quad (49)$$

with

$$\begin{aligned} \dot{\phi} &= -k_1 e + \dot{x}_d - \lambda_1 \chi_1, z = \dot{x} - \phi, \dot{F} = \frac{1}{m_n} \gamma z, \\ \chi_1 &= \int e dt, \chi_2 = \int z dt. \end{aligned} \quad (50)$$

(3) PID-based SMC (PIDSMD) with ESO (PIDSMD + ESO): In [23], a PIDSMD proposed to alleviate chattering phenomenon is given in this paper as

$$\begin{aligned} u_3 = & \frac{1}{T} (\ddot{x}_d + b_n \dot{x}_d + k_n x_d - m_c \dot{e} + b_n \dot{e} + k_n e) - \\ & (P_c q_c + I_c \int q_c dt + D_c \dot{q}_c) - \hat{d}, \end{aligned} \quad (51)$$

with the sliding function  $q_c = m_c e + \dot{e}$ .

The parameters of all the controllers are listed in **Table 1**. It should be noted that the parameters of the controllers are determined first in a preliminary initialization by the simulation results, and subsequently are tuned elaborately and carefully by an iterative trial and error method to get the proper anticipated performance (for each specified controller) on the actual experimental platform. This ensures that the comparison of outcomes achieved are suitably fair, as each specified controller has essentially been appropriately and properly tuned.

**Table 1**  
Parameters of controllers.

Controller	Notation	Value
PID + ESO	$K_p, K_i, K_d$	40.5, 160, 0.1
AIBC + ESO	$k_1, k_2, \lambda_1, \lambda_2, \gamma$	1000, 300, 1000, 1000, 0.1
PIDSMD + ESO	$m_c, P_c, I_c, D_c$	80, 0.15, 120, 0.01
ITSMAIBC	$k_1, k_2, \alpha, \lambda_1, \lambda_2, \xi_1, \xi_2, \gamma, \kappa$	10, 2000, 0.8, 600, 500, 600, 500, 0.1, 0.1

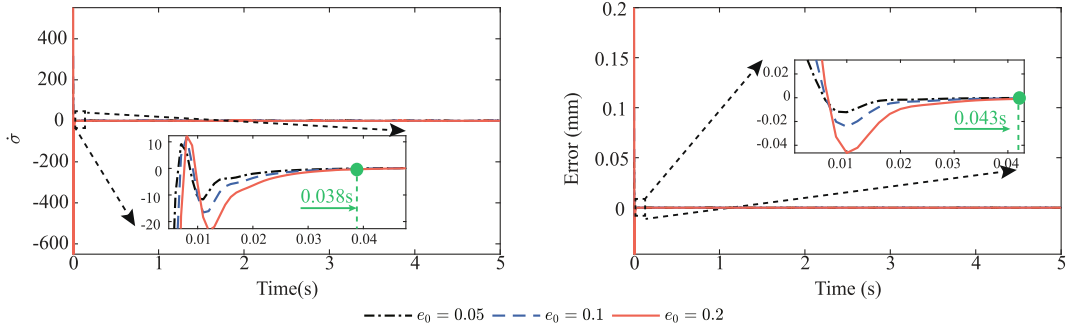


**Fig. 6.** Simulation results of the finite-time convergence performance.

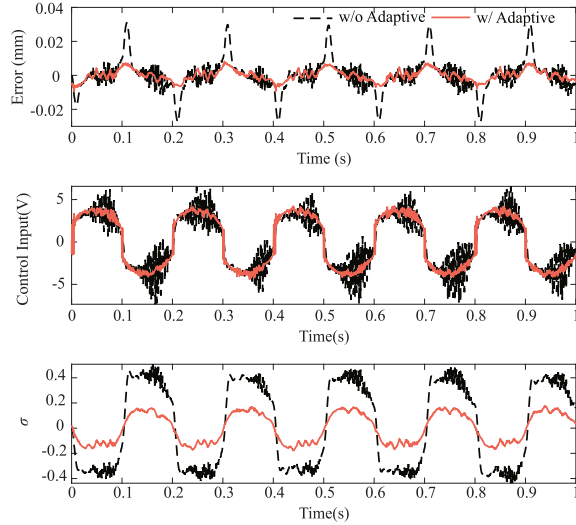


**Fig. 7.** Tracking results with and without adaptive law for 5 Hz sinusoidal wave.

#### 4.3. Performance analysis

Based on the given parameters in Table 1 and nominal plant (47), the finite-time convergence performance of the proposed method is tested by a set of simulations considering a clear expression. To obtain the convergence time, three 1 Hz sinusoidal waves with different initial errors, i.e.  $e_0 = 0.05$  mm, 0.1 mm and 0.2 mm, are input as the references respectively. The time derivative of  $\sigma$  and tracking errors are demonstrated in Fig. 6. It is clear that the convergence time of  $\dot{\sigma}$  increase with  $e_0$ , and the approximate time with  $\dot{\sigma} = 0$  is 0.038s for all the three conditions, i.e.  $T_r = 0.038$  according to Theorem 2. Furthermore, once during the sliding motion, the error  $e$  will converge in a finite time  $T_s$ , which are calculated as 0.0137s, 0.0158s, 0.0181s with the Eq. (15), respectively. Therefore, the total convergence time  $T_f$  are approximate as 0.0517s, 0.0508s, and 0.0538s, respectively. From Fig. 6, it is evident that convergence time of tracking error is about 0.043s for all the three conditions, and is also within the calculated  $T_f$ , which demonstrates the finite-time convergence performance of the proposed method.

The effectiveness of the adaptive law is checked by the 5 Hz sinusoidal wave with 2 mm amplitude as the reference input, and the experimental results are plotted in Fig. 7. It is evident that the performance with adaptive law is better, and at the position suffering from significant friction, the fixed switch gain 20 generates the chattering on the control force and sliding function  $\sigma$ . Moreover, the  $\sigma$  with adaptive law is smaller than that without adaptive law so that the chattering is further alleviated. The above results demonstrate the adaptive law can reduce the chattering phenomenon and improve the tracking performance effectively.

## 5. Results and discussions

### 5.1. Tracking results of continuous sinusoidal waves

The tracking performance for continuous sinusoidal waves is tested firstly with different controllers. It should be noted that the experiments are performed with the toolset on the PUM to accord with the working condition. The references (Ref)

are set as 1 Hz, 5 Hz, and 10 Hz with the tracking amplitude of 2 mm. The tracking results are demonstrated in Figs. 8–10, respectively, and all the statistical results of the motion tracking errors for sinusoidal waves are listed in Table 2. For low-frequency tracking at 1 Hz in Fig. 8, it is clear that the friction is obvious from the zoomed-in view of the plot. Although the ESO is added for the benchmark controllers, the proposed ITSMAIBC achieves the best performance with the root-mean-square error ( $e_{rms}$ ) of 0.0012 mm and maximal error ( $e_{max}$ ) of 0.0055 mm, without any extra state or disturbance observer. For a high-frequency tracking, PID + ESO gets the worst results for the limited bandwidth of PID leading to a large deviation from the reference, although the parameters have been optimized by LQR. For the AIBC + ESO and PIDSMC + ESO, the former one gets slightly improvement than the latter one, although the two methods are totally different. In comparison with

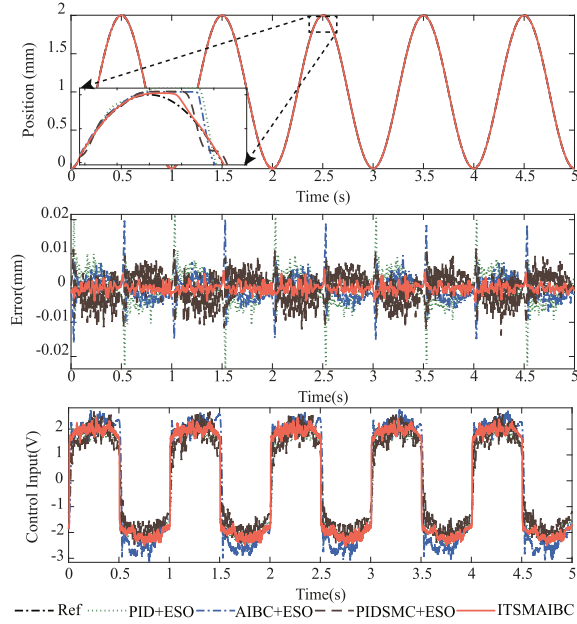


**Fig. 8.** Experimental position tracking results of different controllers at 1 Hz sinusoidal wave.

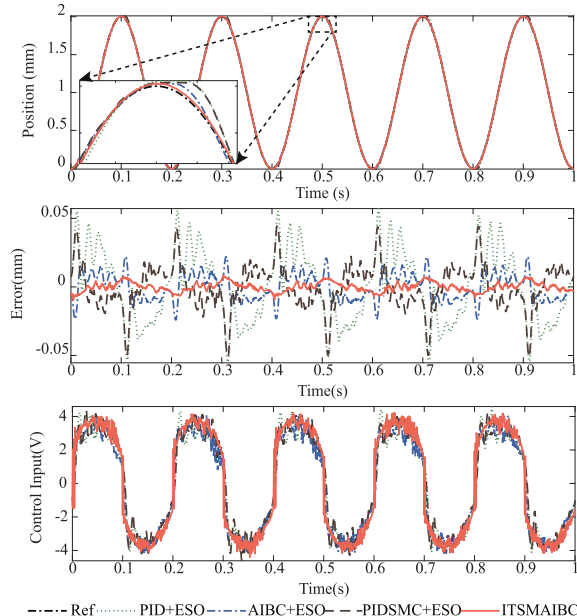


**Fig. 9.** Position tracking results of different controllers at 5 Hz sinusoidal wave.

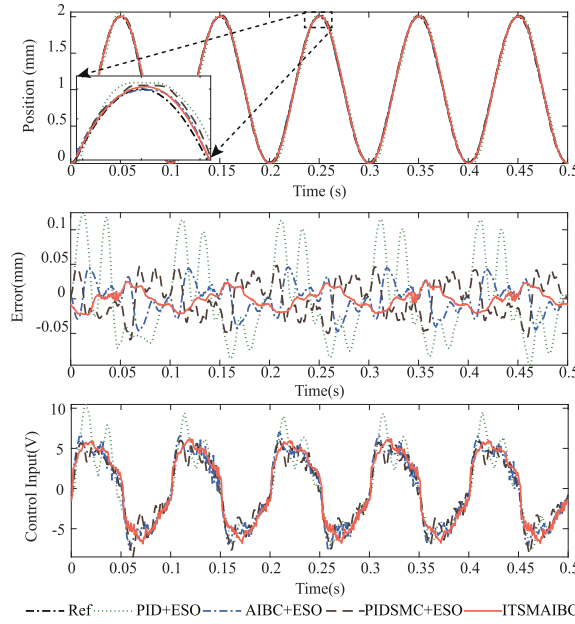


**Fig. 10.** Position tracking results of different controllers at 10 Hz sinusoidal wave.

**Table 2**  
Statistical Results of Tracking Errors of sinusoidal waves.

Statistical Errors (mm)		1 Hz	5 Hz	10 Hz
PID + ESO	$e_{rms}$	0.0051	0.0266	0.0591
	$e_{max}$	0.0236	0.0571	0.1248
AIBC + ESO	$e_{rms}$	0.0037	0.0100	0.0233
	$e_{max}$	0.0201	0.0241	0.0479
PIDSMC + ESO	$e_{rms}$	0.0041	0.0165	0.0267
	$e_{max}$	0.0138	0.0511	0.0596
ITSMAIBC	$e_{rms}$	0.0012	0.0033	0.0127
	$e_{max}$	0.0055	0.0095	0.0266

AIBC + ESO at 5 Hz, the proposed ITSMAIBC achieves the  $e_{rms}$  with 0.0033 mm and  $e_{max}$  with 0.0095 mm, improving by 67% and 60.58%, respectively. The control force for 1 Hz and 5 Hz are similar for the four controllers except for the peak position of the references, where the friction is obvious for the change of motion direction. It is clear that the control force with ITSMAIBC presents less chattering, and consumes less energy but with the best performance.

For the 10 Hz tracking, the heat disturbance is significant for the fast motion between the slider and stator. It also can be observed that the control force of PID + ESO is nearly unstable so that the controller cannot track the high-frequency signal. Under this condition, the proposed controller still gets the best performance among the four controllers with the  $e_{rms}$  at 0.0127 mm and  $e_{max}$  at 0.0266 mm, which are 0.63% and 1.33% of the reference stroke. The key difference between AIBC + ESO and ITSMAIBC lies in that AIBC + ESO is designed based on position errors directly, whereas the proposed method utilizes the integral terminal sliding function so that the precision is improved significantly.

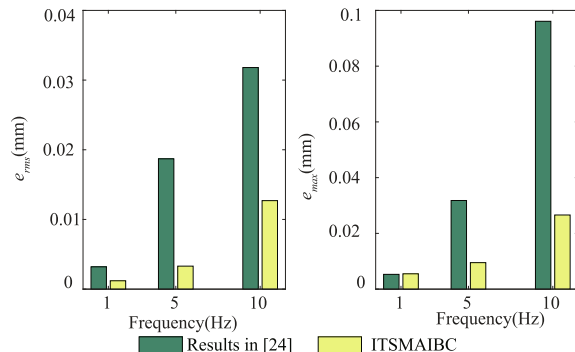


**Fig. 11.** Comparative results with the previous work in [24].

**Fig. 11** shows the comparative results with our previous work in [24], where the nonlinear observer, SMC, and robust adaptive control are mixed together to improve the tracking performance for the same PUM system. It is clear that a more than 50% improvement is achieved by implementing the sole ITSMAIBC without any observer. The above results verify that the proposed method can precisely track the continuous sinusoidal waves with different frequencies.

The performance of the different controllers for 5 Hz sinusoidal waves with different amplitudes are given in **Fig. 12**, where only the  $e_{rms}$  are calculated considering a clear expression. With the increase of amplitude, the performance of PID + ESO and PIDSMC are deteriorated most significantly, especially for the amplitude at 4 mm. The  $e_{rms}$  of the proposed method varies from 0.0027 mm to 0.0041 mm, which shows the adaptability and precision tracking for different amplitudes of sinusoidal waves.

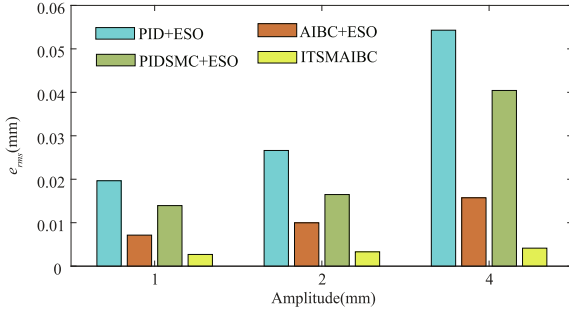


**Fig. 12.** Comparative results of  $e_{rms}$  for 5 Hz sinusoidal waves with different amplitudes.

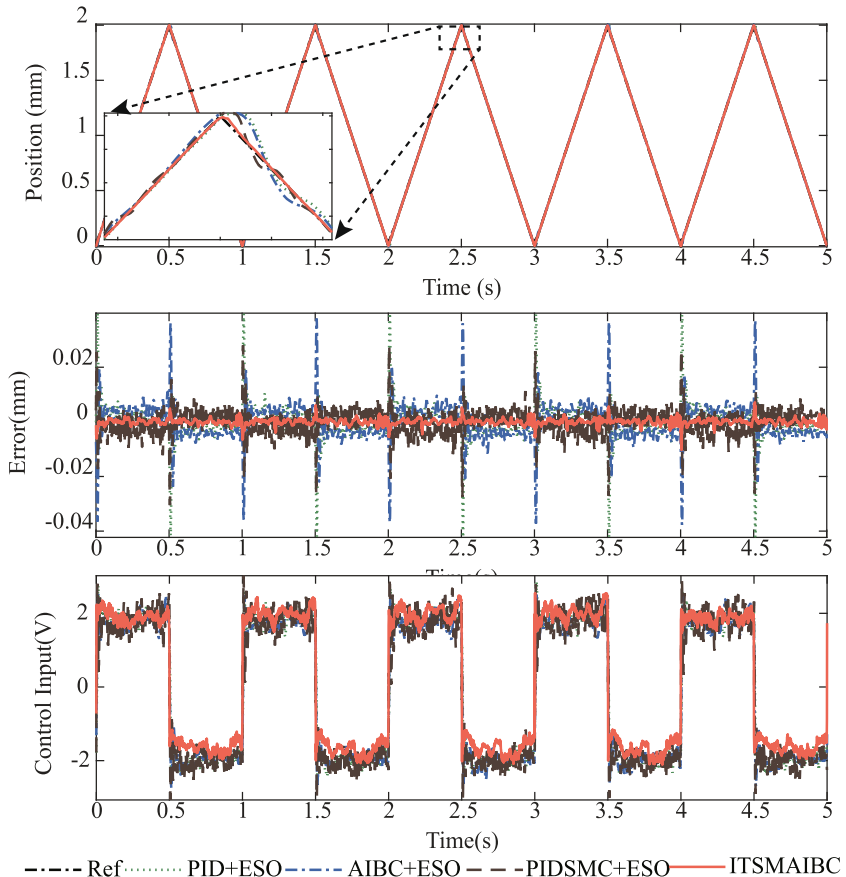


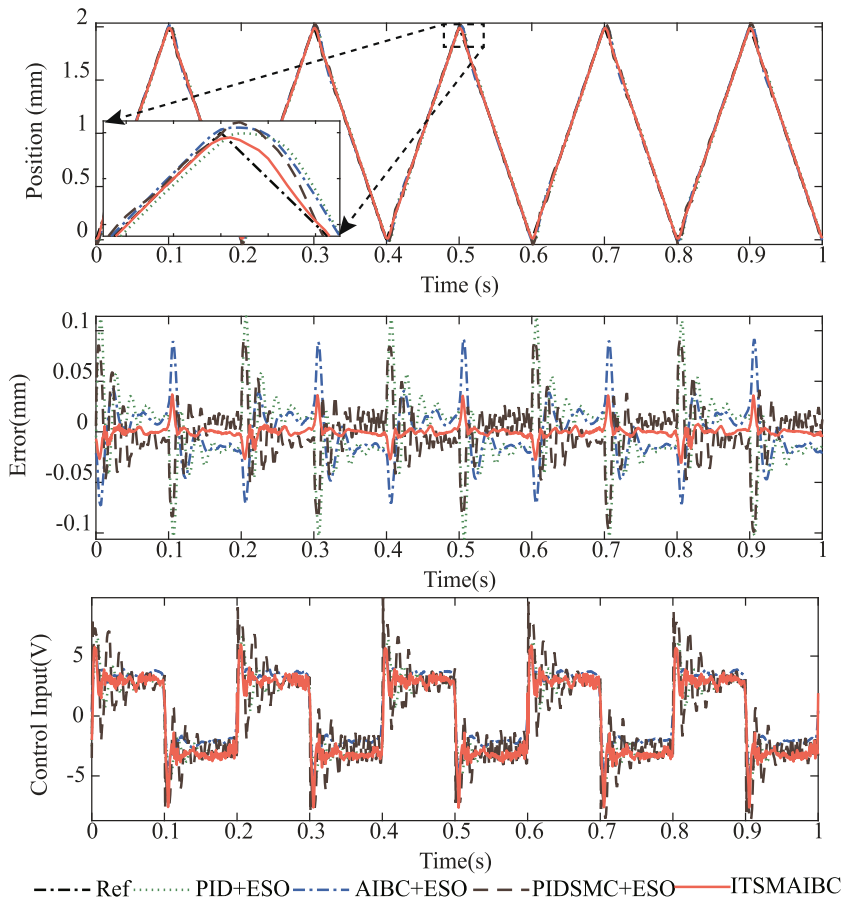
**Fig. 13.** Position tracking results of different controllers at 1 Hz triangular wave.

## 5.2. Tracking results of discontinuous triangular waves

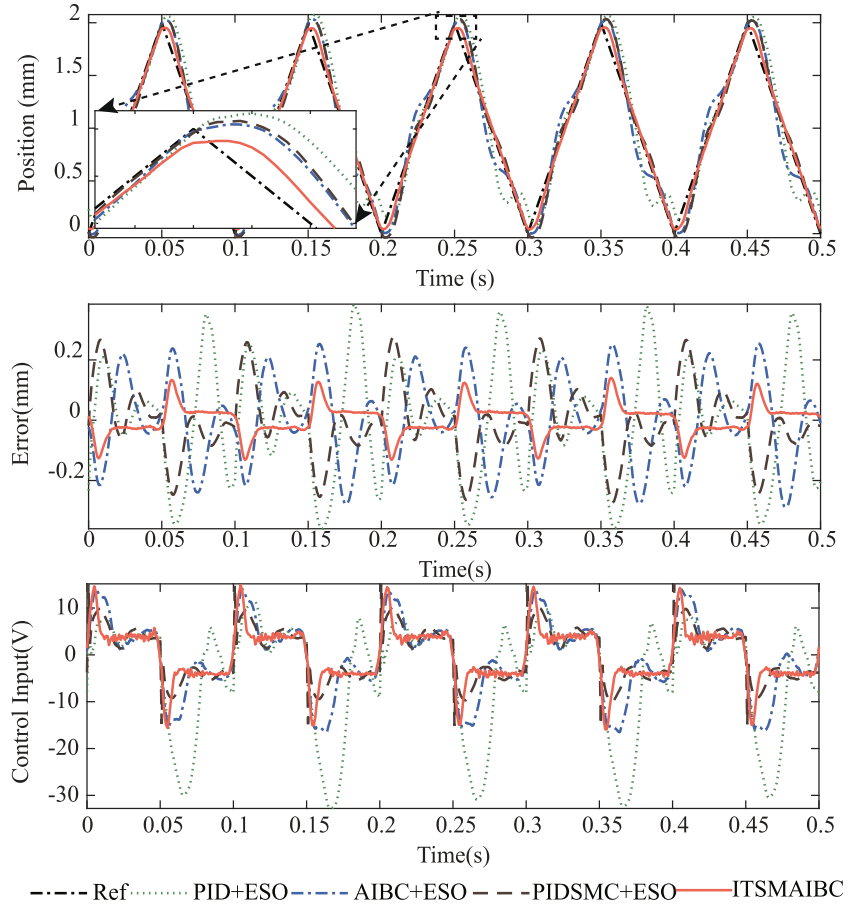
To check the tracking performance for discontinuous signals, the triangular waves are employed in this paper. Except for the inherent disturbance, such as friction, hysteresis, another difficulty to track triangular wave is the high-frequency harmonics of the fundamental frequency, which requires the controller to provide sufficient tracking bandwidth in order to obtain anticipated performance. In this subsection, three types of triangular waves with fundamental frequencies of 1 Hz, 5 Hz, and 10 Hz are applied on different controllers, and the amplitudes are set to the same as 2 mm. The tracking performance, as well as the tracking errors, is shown in Fig. 13–15, respectively. Moreover, Table 3 gives the statistical results for different controllers under various frequencies.

For the 1 Hz tracking results, the  $e_{rms}$  are close to the results of the sinusoidal wave. However, the  $e_{max}$  increase a lot for the discontinuous waves. Despite that, the  $e_{max}$  of ITSMAIBC is 0.0103 mm, only 0.52% of the tracking stroke. For the performance of 5 Hz and 10 Hz, the results of PID + ESO are with the largest errors for the lowest bandwidth and thus PID + ESO cannot deal with the tracking of discontinuous signals well. At 5 Hz, the  $e_{rms}$  are 0.0273 mm, 0.0285 mm, 0.0072 mm for the other three controllers, and the  $e_{max}$  are 0.0919 mm, 0.0993 mm, 0.0370 mm, respectively. Obviously, the performance is improved more than 2.5 times through the proposed ITSMAIBC. For a higher frequency at 10 Hz, the best performance is obtained by the proposed method with the  $e_{rms}$  at 0.0495 mm and  $e_{max}$  at 0.1406 mm. Despite the fact that the performance with ITSMAIBC is degraded significantly in comparison with the results of 10 Hz sinusoidal wave, the conclusion that ITSMAIBC with the largest tracking bandwidth is still verified through this experiment under the same condition. Furthermore, from the control input of the different controllers, an essential pertinent key observation can also be obtained that the proposed method presents less chattering and consumes less energy; and yet still achieves suitably fast and precision tracking of triangular waves. According to the above discussions, it is shown that the proposed controllers can achieve accurate motion tracking of discontinuous triangular waves effectively.

The performance of the different controllers for 5 Hz triangular waves with different amplitudes are given in Fig. 16. It should be noted for the high-frequency harmonics of triangular waves so that the control force is larger than the same frequency's sinusoidal waves. Therefore, the maximum amplitude 2.5 mm is chosen for triangular waves considering the limits

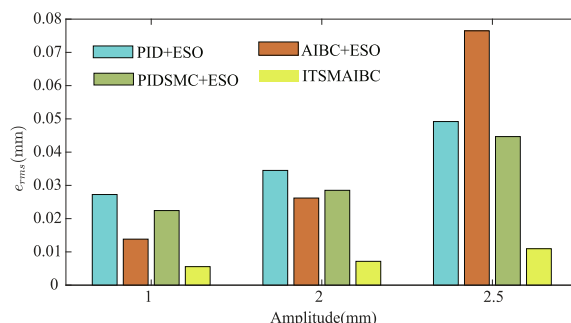


**Fig. 14.** Position tracking results of different controllers at 5 Hz triangular wave.

**Fig. 15.** Position tracking results of different controllers at 10 Hz triangular wave.**Table 3**

Statistical Results of Tracking Errors of triangular waves.

Statistical Errors (mm)		1 Hz	5 Hz	10 Hz
PID + ESO	$e_{rms}$	0.0065	0.0345	0.1849
	$e_{max}$	0.0423	0.1142	0.3851
AIBC + ESO	$e_{rms}$	0.0070	0.0273	0.1382
	$e_{max}$	0.0378	0.0919	0.2891
PIDSMC + ESO	$e_{rms}$	0.0047	0.0285	0.1158
	$e_{max}$	0.0305	0.0993	0.2778
ITSMAIBC	$e_{rms}$	0.0011	0.0072	0.0495
	$e_{max}$	0.0103	0.0370	0.1406

**Fig. 16.** Comparative results of  $e_{rms}$  for 5 Hz triangular waves with different amplitudes.

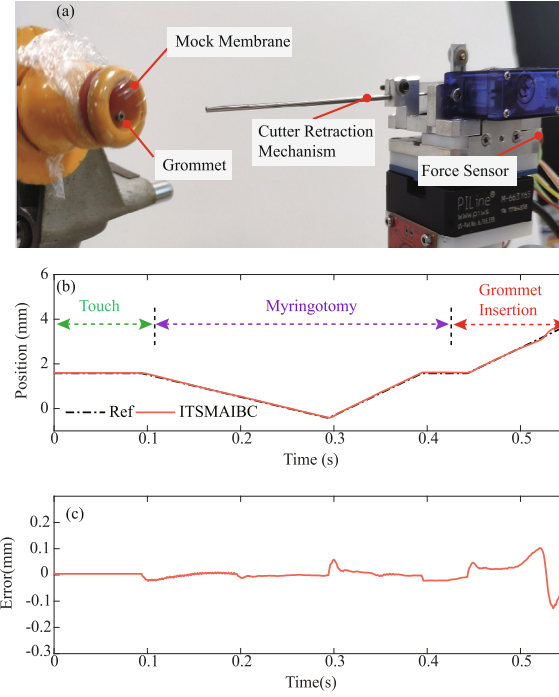


**Fig. 17.** Experimental results of the surgical operation on mock membrane with the proposed method. (a) Experimental setup. (b) Tracking results of the overall surgical operation. (c) Tracking error.

of input voltage of the system. Note that for the tracking results at 2.5 mm, the performance of AIBC + ESO is the worst because the calculated control input exceeds the limits of PUM so that the error increases significantly. In comparison, the  $e_{rms}$  of the proposed method varies from 0.0055 mm to 0.0109 mm, which shows the adaptability and precision tracking for different amplitudes of triangular waves.

### 5.3. Surgical operation on mock membrane

The effectiveness of the proposed controller is also validated on the developed PUM-based surgical device, Ventilation Tube Applicator (VTA), for the treatment of Otitis Media with Effusion (OME) [35]. The whole experimental setup is shown in Fig. 17(a), where the force sensor (FS1500NS, Honeywell) is installed to measure the contact force and guide the sequential actions, and the cutter retraction mechanism is used to cut the mock membrane. To imitate the property of human tympanic membrane, the soft Polyethylene (PE) film is used as the mock membrane [7]. The goal of the surgical operation is to insert a grommet on mock membrane to relieve the pressure from the middle ear. The overall procedures start from the motion of PUM with the cutter retraction mechanism until the contact force with the mock membrane up to 0.03 N. Then, the myringotomy (about 0.35 s) is conducted and the cutter is driven by the cutter retraction mechanism to make an incision on the mock membrane. Finally, the tube insertion (about 0.138 s) is processed, i.e. the cutter is retracted and the grommet is pushed into the mock membrane by the device. The generated motion sequences and the tracking results of the proposed controller are plotted in Fig. 17(b). It is clear the proposed ITSMAIBC tracks the trajectory precisely enough to complete the surgical operation successfully without over-insertion or under-insertion as is shown in Fig. 17(a). It should be also noted that during the myringotomy and tube insertion, the PUM suffers from the time-varying disturbances generated from the force in contact with mock membrane. The tracking error is also given in Fig. 17(c), where the  $e_{max}$  and  $e_{rms}$  are 0.1273 mm and 0.0290 mm, respectively. The above results demonstrate that the tracking performance of the proposed method can complete the surgical operation successfully and precisely in a short time.

## 6. Conclusions

In this paper, the ITSMAIBC is developed for a PUM to achieve precision motion tracking at the presence of inherent friction, hysteresis nonlinearity, heat disturbance, and model uncertainties. The finite-time convergence and accurate tracking performance of the desired reference are guaranteed by an integral-type terminal sliding manifold. Through constructing the second-order differential equations based on the sliding function for controller design, a high-order SMC-like property with less chattering is achieved. Furthermore, the robustness to the unknown disturbance is obtained by the integral backstepping methodology and an adaptive law is designed in order to estimate the upper bound of total disturbance. The overall

ITSMAIBC is deduced by the Lyapunov theory with stability analysis. Comparative experiments are conducted on a PUM system to verify the performance of the proposed controller. For continuous sinusoidal waves up to 10 Hz, the  $e_{rms}$  and  $e_{max}$  are within 0.013 mm and 0.027 mm, i.e., 0.65% and 1.35% of the amplitude at 2 mm. For discontinuous triangular waves, the ITSMAIBC also achieves the best performance in comparison with the other three benchmark controllers under different frequencies and amplitudes. The experimental results verify that the proposed control scheme is simple for practical implementation without any observer, and it can address the adverse impacts effectively as well as realize precision motion for various references. The successful implementation for the surgical operation on mock membrane also indicates the practical value on the application for surgical device.

## Declaration of Competing Interest

The authors declare that they have no known competing financial interests or personal relationships that could have appeared to influence the work reported in this paper.

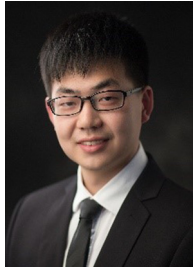
## Acknowledgments

This work was mainly supported by the Biomedical Engineering Programme (BEP) of the Science and Engineering Research Council (SERC), Singapore [SERC Grant No. 132 148 0014], in part by National Nature Science Foundation of China [Grant No. 51375349], and in part by China Scholarship Council (CSC) [Grant No. 201806270142].

## References

- [1] J. Keighobadi, M. Hosseini-Pishrobat, J. Faraji, A. Oveisi, T. Nestorović, Robust nonlinear control of atomic force microscope via immersion and invariance, *Int. J. Robust Nonlinear Control* 29 (4) (2019) 1031–1050.
- [2] Y. Wei, Q. Xu, Design and testing of a new force-sensing cell microinjector based on soft flexure mechanism, *IEEE Sens. J.* 19 (15) (2019) 6012–6019.
- [3] Z. Zhu, H. Du, R. Zhou, P. Huang, W. Zhu, P. Guo, Design and trajectory tracking of a nanometric ultra-fast tool servo, *IEEE Trans. Ind. Electron.* doi: <https://doi.org/10.1109/TIE.2019.2896103>.
- [4] Z. Feng, J. Ling, M. Ming, X.-H. Xiao, High-bandwidth and flexible tracking control for precision motion with application to a piezo nanopositioner, *Rev. Sci. Instrum.* 88 (8) (2017) 085107.
- [5] L. Wang, W. Chen, J. Liu, J. Deng, Y. Liu, A review of recent studies on non-resonant piezoelectric actuators, *Mech. Syst. Signal Process.* 133 (2019) 106254.
- [6] S.-T. Ho, S.-J. Jan, A piezoelectric motor for precision positioning applications, *Precis. Eng.* 43 (2016) 285–293.
- [7] C. Ng, W. Liang, C.W. Gan, H.Y. Lim, K.K. Tan, Optimization of the penetrative path during grommet insertion in a robotic ear surgery, *Mechatronics* 60 (2019) 1–14.
- [8] S. Shi, Z. Huang, J. Yang, Y. Liu, W. Chen, K. Uchino, Development of a compact ring type mdof piezoelectric ultrasonic motor for humanoid eyeball orientation system, *Sens. Actuat. A: Phys.* 272 (2018) 1–10.
- [9] W. Liang, J. Ma, C. Ng, Q. Ren, S. Huang, K.K. Tan, Optimal and intelligent motion control scheme for an ultrasonic-motor-driven xy stage, *Mechatronics* 59 (2019) 127–139.
- [10] M. Ming, Z. Feng, J. Ling, X.-H. Xiao, Hysteresis modelling and feedforward compensation of piezoelectric nanopositioning stage with a modified bouc-wen model, *Micro Nano Lett.* 13 (8) (2018) 1170–1174.
- [11] Z. Li, J. Shan, U. Gabbert, Inverse compensator for a simplified discrete Preisach model using model-order reduction approach, *IEEE Trans. Industr. Electron.* 66 (8) (2018) 6170–6178.
- [12] M. Al Janaideh, O. Aljanaideh, Further results on open-loop compensation of rate-dependent hysteresis in a magnetostrictive actuator with the Prandtl-Ishlinskii model, *Mech. Syst. Signal Process.* 104 (2018) 835–850.
- [13] E. Pennestrì, V. Rossi, P. Salvini, P.P. Valentini, Review and comparison of dry friction force models, *Nonlinear Dyn.* 83 (4) (2016) 1785–1801.
- [14] J. Yao, W. Deng, Z. Jiao, Adaptive control of hydraulic actuators with lugre model-based friction compensation, *IEEE Trans. Industr. Electron.* 62 (10) (2015) 6469–6477.
- [15] K. Jankowski, A. Saha, A. Stefański, Introduction of novel model of friction and analysis of presliding domain of friction with non-local memory effect based upon Maxwell slip model structures, *Tribol. Int.* 102 (2016) 378–391.
- [16] S. Huang, W. Liang, K.K. Tan, Intelligent friction compensation: a review, *IEEE/ASME Trans. Mechatron.* doi: <https://doi.org/10.1109/TMECH.2019.2916665..>
- [17] Y.-J. Wu, G.-F. Li, Adaptive disturbance compensation finite control set optimal control for PMSM systems based on sliding mode extended state observer, *Mech. Syst. Signal Process.* 98 (2018) 402–414.
- [18] Z. Feng, J. Ling, M. Ming, X. Xiao, Integrated modified repetitive control with disturbance observer of piezoelectric nanopositioning stages for high-speed and precision motion, *J. Dyn. Syst. Meas. Control* 141 (8) (2019) 081006.
- [19] J.Y. Lau, W. Liang, H.C. Liaw, K.K. Tan, Sliding mode disturbance observer-based motion control for a piezoelectric actuator-based surgical device, *Asian J. Control* 20 (3) (2018) 1194–1203.
- [20] M. Ruderman, M. Iwasaki, Observer of nonlinear friction dynamics for motion control, *IEEE Trans. Industr. Electron.* 62 (9) (2015) 5941–5949.
- [21] J.Y. Lau, W. Liang, K.K. Tan, Motion control for piezoelectric actuator-based surgical device using neural network and extended state observer, *IEEE Trans. Industr. Electron.* 67 (1) (2019) 402–412.
- [22] Q. Xu, Output-based discrete-time sliding mode control for a piezoelectrically actuated system, *Nonlinear Dyn.* 76 (1) (2014) 551–559.
- [23] J.Y. Peng, X.B. Chen, Integrated pid-based sliding mode state estimation and control for piezoelectric actuators, *IEEE/ASME Trans. Mechatron.* 19 (1) (2012) 88–99.
- [24] J.Y. Lau, W. Liang, K.K. Tan, Adaptive sliding mode enhanced disturbance observer-based control of surgical device, *ISA Trans.* 90 (2019) 178–188.
- [25] J.-A. Escareno, M. Rakotondrabe, D. Habineza, Backstepping-based robust-adaptive control of a nonlinear 2-dof piezoactuator, *Control Eng. Practice* 41 (2015) 57–71.
- [26] F.-J. Lin, S.-Y. Lee, P.-H. Chou, Intelligent integral backstepping sliding-mode control using recurrent neural network for piezo-flexural nanopositioning stage, *Asian J. Control* 18 (2) (2016) 456–472.
- [27] Y. Zhang, P. Yan, Sliding mode disturbance observer-based adaptive integral backstepping control of a piezoelectric nano-manipulator, *Smart Mater. Struct.* 25 (12) (2016) 125011.
- [28] Q. Xu, Continuous integral terminal third-order sliding mode motion control for piezoelectric nanopositioning system, *IEEE/ASME Trans. Mechatron.* 22 (4) (2017) 1828–1838.

- [29] Q. Xu, Precision motion control of piezoelectric nanopositioning stage with chattering-free adaptive sliding mode control, *IEEE Trans. Autom. Sci. Eng.* 14 (1) (2016) 238–248.
- [30] V. Utkin, Discussion aspects of high-order sliding mode control, *IEEE Trans. Autom. Control* 61 (3) (2015) 829–833.
- [31] M. Van, M. Mavrovouniotis, S.S. Ge, An adaptive backstepping nonsingular fast terminal sliding mode control for robust fault tolerant control of robot manipulators, *IEEE Trans. Syst., Man, Cybern.: Syst.* 49 (7) (2018) 1448–1458.
- [32] Y. Li, Q. Xu, Adaptive sliding mode control with perturbation estimation and pid sliding surface for motion tracking of a piezo-driven micromanipulator, *IEEE Trans. Control Syst. Technol.* 18 (4) (2009) 798–810.
- [33] A. Al-Ghanimi, J. Zheng, Z. Man, A fast non-singular terminal sliding mode control based on perturbation estimation for piezoelectric actuators systems, *Int. J. Control* 90 (3) (2017) 480–491.
- [34] K. Abidi, J.-X. Xu, Y. Xinghuo, On the discrete-time integral sliding-mode control, *IEEE Trans. Autom. Control* 52 (4) (2007) 709–715.
- [35] K. Kiong Tan, W. Liang, S. Huang, L.P. Pham, S. Chen, C. Wee Gan, H. Yee Lim, Precision control of piezoelectric ultrasonic motor for myringotomy with tube insertion, *J. Dyn. Syst. Measure. Control* 137 (6) (2015).
- [36] H.C. Liaw, B. Shirinzadeh, J. Smith, Robust motion tracking control of piezo-driven flexure-based four-bar mechanism for micro/nano manipulation, *Mechatronics* 18 (2) (2008) 111–120.
- [37] G.-Y. Gu, L.-M. Zhu, C.-Y. Su, H. Ding, S. Fatikow, Modeling and control of piezo-actuated nanopositioning stages: a survey, *IEEE Trans. Autom. Sci. Eng.* 13 (1) (2014) 313–332.
- [38] D. Sabarianand, P. Karthikeyan, T. Muthuramalingam, A review on control strategies for compensation of hysteresis and creep on piezoelectric actuators based micro systems, *Mech. Syst. Signal Process.* 140 (2020) 106634.
- [39] H. Wang, Z. Han, Q. Xie, W. Zhang, Finite-time chaos synchronization of unified chaotic system with uncertain parameters?, *Commun. Nonlinear Sci. Numer. Simul.* 14 (5) (2009) 2239–2247.
- [40] J. Khawwaf, J. Zheng, R. Chai, R. Lu, Z. Man, Adaptive microtracking control for an underwater ipmc actuator using new hyperplane-based sliding mode, *IEEE-ASME Trans. Mechatronics* 24 (5) (2019) 2108–2117.
- [41] Y. Feng, X. Yu, Z. Man, Non-singular terminal sliding mode control of rigid manipulators, *Automatica* 38 (12) (2002) 2159–2167.
- [42] P. Ioannou, *Adaptive control tutorial*, SIAM, 2006.
- [43] J. Ling, M. Rakotondrabe, Z. Feng, M. Ming, X. Xiao, A robust resonant controller for high-speed scanning of nanopositioners: design and implementation, *IEEE Trans. Control Syst. Technol.* doi: <https://doi.org/10.1109/TCST.2019.2899566>.
- [44] G. Wang, Q. Xu, Adaptive terminal sliding mode control for motion tracking of a micropositioning system, *Asian J. Control* 20 (3) (2018) 1241–1252.
- [45] B. Ahi, M. Haeri, Linear active disturbance rejection control from the practical aspects, *IEEE/ASME Trans. Mechatron.* 23 (6) (2018) 2909–2919.



**Zhao Feng** received the B.S degrees in Mechanical Engineering from School of Power and Mechanical Engineering, Wuhan University, Wuhan, China in 2010. He is currently pursuing the Ph.D. degree in Mechanical Engineering at Wuhan University, Wuhan, China. He is now as a visiting Ph. D student at the Department of Electrical and Computer Engineering, National University of Singapore. His research interests include vibration control, iterative learning control, nanopositioning and robotics.



**Wenyu Liang** (M'14) received the B.Eng. and M.Eng. degrees in mechanical engineering from the China Agricultural University, Beijing, China, in 2008 and 2010, respectively, and the Ph.D. degree in electrical and computer engineering from the National University of Singapore, Singapore, in 2014. He is currently an Adjunct Assistant Professor with the Department of Electrical and Computer Engineering, National University of Singapore. His research interests mainly include robotics, mechatronics and automatic, precision motion control and force control with applications in medical and industrial technology.



**Jie Ling** received his B.S. and Ph.D. degrees in Mechanical Engineering from School of Power and Mechanical Engineering, Wuhan University, China, in 2012 and 2018, respectively. He was a joint Ph.D. student with Department of Automatic Control and Micro-Mechatronic Systems, FEMTO-st Institute, France in 2017. From 2019 to 2020, he is a joint Postdoc Researcher with Department of Biomedical Engineering, National University of Singapore, Singapore. Since 2018, he has been a Postdoctoral Researcher with Department of Mechanical Engineering, Wuhan University, Wuhan, China. His research interests include mechanical design and precision motion control of nanopositioning stages and micromanipulation robots.



**Xiaohui Xiao** received the B. S. and M.S. degrees in Mechanical Engineering from Wuhan University, Wuhan, China, in 1991 and 1998, respectively, and the Ph.D. degree in mechanical engineering from Huazhong University of Science and Technology, Wuhan, China, in 2005. She joined the Wuhan University, Wuhan, China, in 1998, where she is currently a Full Professor with the Mechanical Engineering Department, School of Power and Mechanical Engineering. Her current research interests include mobile robotics, high-precision positioning control, and signal processing.



**Kok Kiong Tan** (S'94-M'99) received the B.Eng. and Ph.D. degrees in electrical and computer engineering from the Department of Electrical and Computer Engineering, National University of Singapore, Singapore, in 1992 and 1995, respectively. Prior to joining the National University of Singapore, he was a Research Fellow with the Singapore Institute of Manufacturing Technology, Singapore, a national R&D institute spearheading the promotion of R&D in local manufacturing industries, where he was involved in managing industrial projects. He was a Professor with the National University of Singapore. He has authored or coauthored more than 200 journal papers to date and has written 14 books, all resulting from research in these areas. His current research interests include precision motion control and instrumentation, advanced process control and auto-tuning, and general industrial automation.



**Tong Heng Lee** (M'90) received the B.A. degree (First Class Hons.) in engineering tripos from Cambridge University, Cambridge, U.K., in 1980, and the Ph.D. degree in electrical engineering from Yale University, New Haven, CT, USA, in 1987. He is currently a Professor with the Department of Electrical and Computer Engineering, National University of Singapore, Singapore. His research interests are in the areas of adaptive systems, knowledge-based control, intelligent mechatronics and computational intelligence. He currently holds Associate Editor appointments in many flagship journals such as the IEEE Transactions in Systems, Man and Cybernetics; the Control Engineering Practice (an IFAC journal); and the International Journal of Systems Science (Taylor and Francis, London). In addition, he is the Deputy Editor-in-Chief of IFAC Mechatronics journal. He has also co-authored five research monographs (books), and holds four patents (two of which are in the technology area of adaptive systems, and the other two are in the area of intelligent mechatronics). He was an Invited Panelist, an Invited Keynote Speaker for many international conferences. He was a recipient of the Cambridge University Charles Baker Prize in Engineering and several best conference paper prizes. He was also a multiple winner of the National University of Singapore FoE Engineering Educator Award, and is now on the Engineering Educator Honour Roll.